Vison Crystals in an Extended Kitaev Model on the Honeycomb Lattice

Shang-Shun Zhang,[1] Zhentao Wang,[1] Gábor B. Halász,[2] and Cristian D. Batista[1,3]
[1]Department of Physics and Astronomy, The University of Tennessee, Knoxville, Tennessee 37996, USA
[2]Materials Science and Technology Division, Oak Ridge National Laboratory, Oak Ridge, Tennessee 37831, USA
[3]Neutron Scattering Division and Shull-Wollan Center, Oak Ridge National Laboratory, Oak Ridge, Tennessee 37831, USA

(Received 6 March 2019; published 31 July 2019)

We introduce an extension of the Kitaev honeycomb model by including four-spin interactions that preserve the local gauge structure and, hence, the integrability of the original model. The extended model has a rich phase diagram containing five distinct vison crystals, as well as a symmetric π-flux spin liquid with a Fermi surface of Majorana fermions and a sequence of Lifshitz transitions. We discuss possible experimental signatures and, in particular, present finite-temperature Monte Carlo calculations of the specific heat and the static vison structure factor. We argue that our extended model emerges naturally from generic perturbations to the Kitaev honeycomb model.

DOI: 10.1103/PhysRevLett.123.057201

Introduction.—The famous Kitaev model on the honeycomb lattice [1] is an exactly solvable yet experimentally realistic model of a quantum spin liquid. In contrast to more conventional magnetic phases, quantum spin liquids retain extensive (quantum) fluctuations all the way down to zero temperature [2], where the spins appear to fractionalize into deconfined "spinon" quasiparticles coupled to appropriate gauge fields [3].

The Kitaev model is approximately realized in a family of strongly spin-orbit-coupled honeycomb materials, where its anisotropic spin interactions emerge between effective $J = 1/2$ angular momenta in the t_{2g} orbitals of $4d$ or $5d$ ions [4–7]. To determine the most accurate microscopic spin models for these Kitaev materials, including $(\mathrm{Na, Li})_2\mathrm{IrO}_3$ [8–16] and α-RuCl_3 [17–30], various extensions of the Kitaev model have been considered and analyzed with a wide range of techniques [31–51]. While these models are experimentally realistic and have rich phase diagrams in the classical limit, it is challenging to identify and characterize quantum phases in them. For a start, the honeycomb lattice may harbor many different quantum spin liquids [52,53], and the Kitaev spin liquid, captured by the Kitaev model, is only one among these many candidates. In addition, a quantum spin liquid may also remain "hidden" by appearing on top of classical symmetry-breaking order [54].

From a more phenomenological point of view, the low-energy physics of the Kitaev spin liquid is described by Majorana fermions (spinons) with Dirac nodes, coupled to an emergent $\mathbb{Z}_2$ gauge field [1]. At each plaquette of the honeycomb lattice, the $\mathbb{Z}_2$ gauge field may form a π flux, corresponding to a "vison" excitation. In turn, the presence of such a vison affects the kinetic energy of the spinons via the Berry phase π picked up by each spinon moving around it. For the pure Kitaev model, the spinons are governed by a nearest-neighbor hopping problem (cf. electrons in graphene), and, due to the lack of frustration, the ground state has no visons at any plaquettes [1,55]. However, if the hopping problem is frustrated by competing hopping amplitudes, the presence of a vison may reduce the frustration and, thus, lower the kinetic energy of the spinons. Such a frustration in the hopping amplitudes is known to stabilize crystals of topological solitons, such as baby skyrmions or merons, in itinerant magnets [56–58], and one may thus expect it to stabilize analogous vison crystals in the Kitaev spin liquid.

In this Letter, we extend the Kitaev model by including four-spin interactions that preserve the exact solution of the model and emerge naturally from generic perturbations. By introducing frustrated further-neighbor hopping for the Majorana fermions, these additional interactions stabilize a rich variety of vison crystals, as well as a symmetric π-flux spin liquid with a vison at every plaquette. Interestingly, the π-flux spin liquid exhibits a Fermi surface of Majorana fermions undergoing two subsequent Lifshitz transitions. On a technical level, we first use a simple variational treatment to compute the zero-temperature phase diagram of our extended model. The validity of this approach is then confirmed by unbiased Monte Carlo (MC) simulations that also reveal the finite melting temperatures of the vison crystals.

Model.—We consider a generalized Kitaev Hamiltonian on the honeycomb lattice:

$$\mathcal{H} = \mathcal{H}_{K_1} + \mathcal{H}_{K_3}, \tag{1}$$

where $\mathcal{H}_{K_1} = -K_1 \sum_{\langle ij\rangle_\alpha} \sigma_i^\alpha \sigma_j^\alpha$ is the usual [1] isotropic Kitaev Hamiltonian with ferromagnetic ($K_1 > 0$) Ising interactions between the spin components σ^α along each $\alpha = \{x, y, z\}$ bond $\langle ij\rangle_\alpha$ [see Fig. 1(a)] and

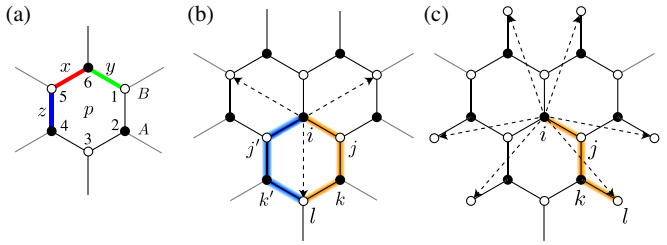

FIG. 1. Extended Kitaev model. (a) Honeycomb lattice with two sublattices A and B (black and white dots), three bond types x, y, and z (red, green, and blue bonds, respectively), and the site-labeling convention around a plaquette p. (b),(c) Representative (orange) paths $\langle ijkl\rangle_{yzx}$ (b) and $\langle ijkl\rangle_{yzy}$ (c) associated with the K_3 and K_3' terms in Eq. (2), respectively; four-spin interactions along such paths give rise to Majorana hopping from any site i to all its third neighbors [59], as indicated by the dashed arrows. For the path $\langle ijkl\rangle_{yzx}$ (b), the symmetry-related path $\langle ij'k'l\rangle_{xzy}$ is marked by blue.

$$\mathcal{H}_{K_3} = K_3 \sum_{\langle ijkl\rangle_{\alpha\beta\gamma}} \sigma_i^\alpha \sigma_j^\gamma \sigma_k^\alpha \sigma_l^\gamma - K_3' \sum_{\langle ijkl\rangle_{\alpha\beta\alpha}} \sigma_i^\alpha \sigma_j^\gamma \sigma_k^\gamma \sigma_l^\alpha, \quad (2)$$

where $(\alpha\beta\gamma)$ is a permutation of (xyz) in each term and $\langle ijkl\rangle_{\alpha\beta\gamma}$ is a path of length 3 consisting of bonds $\langle ij\rangle_\alpha$, $\langle jk\rangle_\beta$, and $\langle kl\rangle_\gamma$. Each term in $\mathcal{H}_{K_3}$ is the product of the three terms in $\mathcal{H}_{K_1}$ that correspond to the three bonds along the appropriate path. Different K_3 and K_3' terms are related by space-group symmetries, simultaneously transforming the lattice and the spins; particular examples of their respective paths, with $(\alpha\beta\gamma) = (yzx)$, are depicted in Figs. 1(b) and 1(c). We remark that, for each path $\langle ijkl\rangle_{\alpha\beta\gamma}$ going around one "half" of a hexagon, connecting opposite vertices i and l, there is a symmetry-related path $\langle lk'j'i\rangle_{\alpha\beta\gamma} = \langle ij'k'l\rangle_{\gamma\beta\alpha}$ going around the other half of the hexagon [see Fig. 1(b)].

Importantly, the exact solution of $\mathcal{H}_{K_1}$ [1] is preserved by the additional terms in Eq. (2). Indeed, since $\mathcal{H}$ commutes with the flux operator $W_p = \sigma_1^x\sigma_2^y\sigma_3^z\sigma_4^x\sigma_5^y\sigma_6^z$ at each plaquette p [see Fig. 1(a)], one can identify static $\mathbb{Z}_2$ flux or vison degrees of freedom at these plaquettes, each being present (absent) if the corresponding W_p takes eigenvalue -1 $(+1)$. Following the Majorana fermionization $\sigma_j^\alpha = ib_j^\alpha c_j$, the Hamiltonian takes the form [60]

$$\mathcal{H} = iK_1 \sum_{\langle ij\rangle_\alpha} u_{ij}^\alpha c_i c_j + iK_3 \sum_{\langle ijkl\rangle_{\alpha\beta\gamma}} u_{ij}^\alpha u_{kj}^\beta u_{kl}^\gamma c_i c_l + iK_3' \sum_{\langle ijkl\rangle_{\alpha\beta\alpha}} u_{ij}^\alpha u_{kj}^\beta u_{kl}^\alpha c_i c_l, \quad (3)$$

where $u_{ij}^\alpha = -u_{ji}^\alpha \equiv ib_i^\alpha b_j^\alpha$ is a $\mathbb{Z}_2$ gauge field along the α bond $\langle ij\rangle_\alpha$. Since these gauge fields are conserved quantities, $u_{ij}^\alpha = \pm 1$, providing a redundant description of the conserved gauge fluxes, $W_p = u_{12}^z u_{32}^x u_{34}^y u_{54}^z u_{56}^x u_{16}^y = \pm 1$, Eq. (3) is quadratic in the Majorana fermions c_i, thus giving rise to free fermion ("spinon") excitations after a straightforward diagonalization [60]. From the perspective of the Majorana fermions, the K_1 terms describe first-neighbor hopping, while the additional K_3 and K_3' terms describe third-neighbor hopping [59].

In analogy with how three-spin interactions may be obtained from a Zeeman field [1], the four-spin interactions in Eq. (2) can, in principle, be generated by a perturbative treatment of Heisenberg and/or symmetric off-diagonal (Γ) interactions on top of the pure Kitaev model. Taking a more universal approach and considering Eq. (3) as an effective low-energy theory for the Majorana fermions [61], we know that generic time-reversal-symmetric perturbations to $\mathcal{H}_{K_1}$ must generate all Majorana terms that are consistent with the projective symmetries of the Kitaev spin liquid [53]. Given that all interaction terms are irrelevant and second-neighbor hopping terms are forbidden by time reversal, Eq. (3) is the most natural effective theory beyond the pure Kitaev model.

Phase diagram.—The ground state of $\mathcal{H}_{K_1}$ belongs to the zero-flux sector, characterized by $W_p = +1$ for all p [1,55]. In the presence of the additional interactions, however, the ground state may belong to a wide range of different flux sectors, as shown by the $T = 0$ phase diagram in Fig. 2. This phase diagram is obtained from a simple variational analysis, by comparing the energies of the seven flux sectors appearing in the diagram on finite lattices of 48×48 unit cells [62]. Furthermore, it is fully consistent with unbiased finite-temperature MC simulations, discussed in a later section [63].

We first concentrate on the two fully symmetric non-crystal phases occupying most of the phase diagram: the

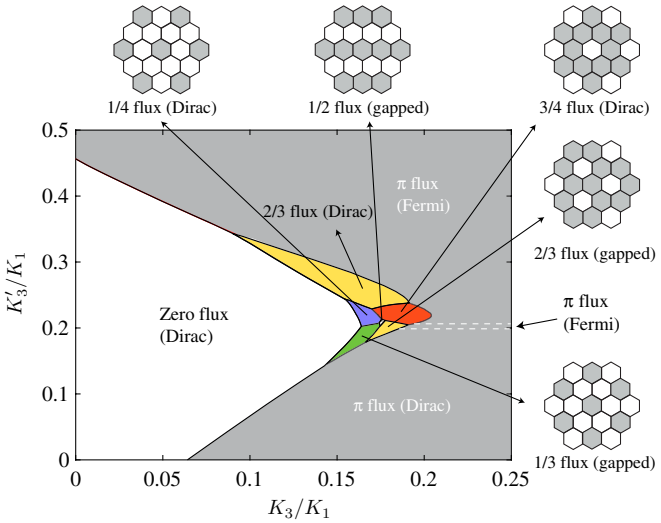

FIG. 2. Phase diagram of the extended Kitaev model. Flux configurations of distinct vison crystals (colored phases) are depicted in separate panels; the presence (absence) of a flux is marked at each plaquette by gray (white) filling.

zero-flux phase, which has no fluxes at any plaquettes, and the π-flux phase, which has a $\mathbb{Z}_2$ flux at each plaquette. For $K_3 = K_3' = 0$, the creation of each $\mathbb{Z}_2$ flux with $W_p = -1$ costs a finite energy $\Delta \approx 0.15K_1$, and the ground state thus belongs to the zero-flux sector. For $K_3/K_1 > 0$, the K_1 and K_3 terms in Eq. (3) give rise to a frustrated Majorana hopping and, hence, an increase in the ground-state energy. However, due to the two paths between any two opposite sites i and l around a plaquette p [see Fig. 1(b)], there are two equivalent hopping terms $\propto iK_3c_ic_l$ in Eq. (3), which interfere constructively for $W_p = +1$ and destructively for $W_p = -1$. Consequently, as K_3/K_1 is increased, fluxes are effective in relieving frustration from the Majorana hopping and, thus, become energetically favorable. Since the effective interaction between nearby fluxes is attractive for small K_3'/K_1 [1], the corresponding phase transition between the zero-flux and the π-flux phases is strongly first order.

Increasing K_3'/K_1, one can modify this interaction and stabilize various intermediate phases with nontrivial flux configurations. Indeed, there are five distinct translation-symmetry-breaking vison-crystal phases in Fig. 2, with their ordering wave vectors $\boldsymbol{Q}$ corresponding to either the K point or the M point(s) of the Brillouin zone (BZ). The two $\boldsymbol{Q} = \boldsymbol{Q}_K$ crystals have supercells of three plaquettes, containing one vison ("1/3 flux crystal") and two visons ("2/3 flux crystal"), respectively. Since there are three different M points, $\boldsymbol{Q} = \boldsymbol{Q}_M$ crystals can exhibit single-$\boldsymbol{Q}$ or multi-$\boldsymbol{Q}$ ordering. The single-$\boldsymbol{Q}$ crystal is a stripy configuration, corresponding to a supercell of two plaquettes containing one vison ("1/2 flux crystal"), while the two triple-$\boldsymbol{Q}$ crystals have supercells of four plaquettes, containing one vison ("1/4 flux crystal") and three visons ("3/4 flux crystal"), respectively.

Majorana problems.—For the different ground-state flux sectors discussed above, distinct configurations of the gauge fields $u_{ij}^{\alpha} = \pm 1$ lead to different Majorana Hamiltonians in Eq. (3). Consequently, each phase in Fig. 2 has its own Majorana band dispersion and a corresponding density of states. The low-energy physics, giving rise to universal signatures in experiments, is determined by the nodal structures of the Majorana fermions. For the zero-flux phase, including the pure Kitaev model, as well as for the 1/4 and 3/4 flux crystals, the Majorana fermions are gapless at Dirac points and, thus, have a linear density of states at low energies. For the 1/3 and 1/2 flux crystals, the Majorana fermions are fully gapped and, thus, have zero density of states below the energy gap. For the 2/3 flux crystal, there are two disconnected phases where the Majorana fermions are gapless at Dirac points and fully gapped, respectively (see Fig. 2).

Interestingly, the Majorana fermions have more complex nodal structures in the π-flux phase. This phase is amenable to a full analytic understanding, as, due to the perfect cancelation of all K_3 terms in Eq. (3), the Majorana problem has only one dimensionless parameter ratio $\kappa \equiv K_3'/K_1$. With a simple calculation [60], we find that there are, in fact, *three* distinct π-flux phases characterized by different Majorana nodal structures.

In particular, there is a π-flux phase where the Majorana fermions are gapless at Dirac points only and another two π-flux phases where these Dirac points coexist with Fermi surfaces (i.e., nodal lines) of distinct topologies (see Fig. 3). The dashed lines in Fig. 2 indicate two subsequent Lifshitz transitions [64] separating these three phases as a function of increasing κ. For $\kappa < 1/5$, the only nodal structures are Dirac points. At the first Lifshitz transition, $\kappa = 1/5$, small pockets of Fermi surfaces appear around these Dirac points and gradually expand as κ is further increased. At the second Lifshitz transition, $\kappa = (\sqrt{2} - 1)/2 \approx 0.207$, these small pockets then connect with each other to form larger pockets. We remark that the Dirac points are located at exactly the same momenta for all values of κ.

Such a coexistence of Dirac points and Fermi surfaces is rather surprising and is not expected to be stable. Instead, due to the nature of the time-reversal and particle-hole symmetries in the Majorana problem [65], one would anticipate only Dirac points to be generically present, as in all the other phases of Fig. 2. Indeed, we find that the Fermi surfaces exist due to the particular simplicity of the problem up to third-neighbor hopping terms [60] and that each Fermi surface is gapped out into six Dirac points

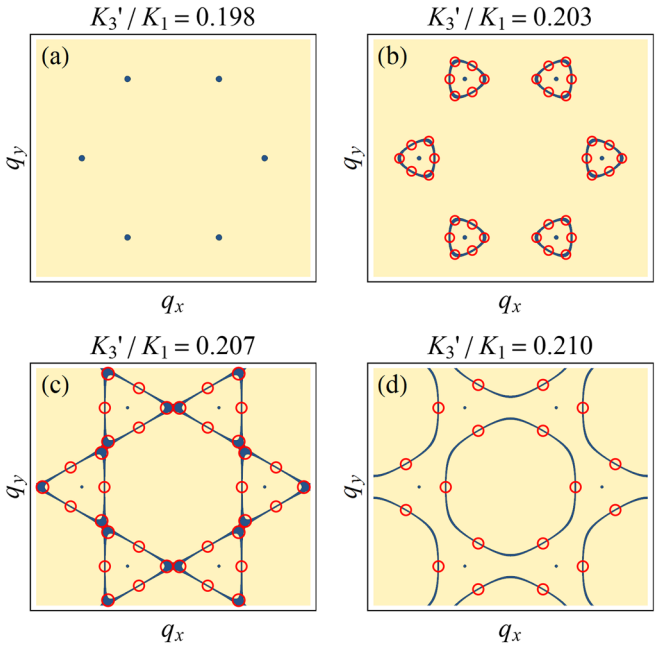

FIG. 3. Majorana nodal structures (dark blue) in the various π-flux phases: the Dirac phase (a), the first Fermi phase (b), the Lifshitz transition between the two Fermi phases (c), and the second Fermi phase (d). In the presence of generic further-neighbor Majorana hopping terms [59], each Fermi surface is gapped out into six Dirac points (red circles).

(see Fig. 3) when generic fifth-neighbor hopping terms [59], respecting the projective symmetries of the system, are included in Eq. (3). However, assuming that such terms are small enough, *approximate* Fermi surfaces are still expected to be observable in experiments.

Experimental signatures.—The phase diagram in Fig. 2 contains a rich variety of phases with all possible Majorana nodal structures in two dimensions, including Fermi surfaces, Dirac points, and fully gapped scenarios. Because of their distinct low-energy physics, these phases are characterized by different experimental signatures. First, we expect the low-temperature specific heat to behave as $C \propto T$ for Fermi phases, $C \propto T^2$ for Dirac phases, and $C \propto e^{-\Delta_v/T}$ for fully gapped phases, where the activated behavior should be controlled by the vison gap Δ_v, as it is actually smaller than the Majorana gap. Second, the various Majorana nodal structures may be distinguished by their low-energy fingerprints in spectroscopic probes, such as resonant inelastic x-ray scattering [66,67]. Third, the Majorana Fermi surface in the π-flux phase leads to impurity-induced Friedel oscillations in the magnetic energy density [60]. In turn, such magnetic Friedel oscillations should be measurable with nuclear magnetic resonance (NMR), as they induce an oscillatory bond-length modulation via magnetostriction.

For the vison-crystal phases in Fig. 2, the spontaneous breaking of translation symmetry leads to further experimental signatures. First of all, due to magnetostriction, each vison crystal generates a characteristic bond-length modulation throughout the lattice, which can be picked up with NMR or elastic x-ray scattering. Moreover, the enlarged unit cell results in a larger number of distinct bands for the Majorana fermions, and, therefore, in contrast to the pure Kitaev model [68,69], the dynamical spin structure factor [60], directly measurable by inelastic neutron scattering, has multiple peaks as a function of the energy (see Fig. 4). Finally, unlike the fully symmetric phases, each vison-crystal phase has a finite-temperature phase transition at a critical temperature T_c.

Monte Carlo simulations.—To verify the phase diagram in Fig. 2 and to extract the melting temperatures T_c of the vison crystals, we perform MC simulations of $\mathcal{H}$ based on a Metropolis algorithm to update the "classical" $\mathbb{Z}_2$ fields $\{u_{ij}^{\alpha} = \pm 1\}$. The energy of each field configuration is computed by diagonalizing the quadratic Majorana Hamiltonian in Eq. (3) [70,71] on $L \times L$ lattices with $L = \{6, 12, 18\}$ [60]. For each temperature, a single run contains 10 000 MC sweeps for equilibration and another 20 000 MC sweeps for measurement [72].

Figure 5 shows our results for the heat capacity $C(T)$ and the static vison structure factor,

$$\rho_v(\boldsymbol{k}) = \frac{1}{L^2}\sum_{p,p'} e^{i\boldsymbol{k}\cdot(\boldsymbol{X}_p - \boldsymbol{X}_{p'})}\langle W_p W_{p'}\rangle, \tag{4}$$

for representative parameters of four different vison crystals, where $\boldsymbol{X}_p$ is the position of plaquette p and $\boldsymbol{k}$ is the ordering wave vector of each vison crystal, corresponding to either the K or the M point of the BZ. We first observe that, as for the pure Kitaev model, $C(T)$ exhibits both a high- and a low-temperature peak, which correspond to spinon and vison excitations, respectively [70,71]. However, the low-temperature peak signals the onset of vison-crystal ordering at $T = T_c$, as confirmed by the sharp growth of the corresponding Bragg peak in $\rho_v(\boldsymbol{k})$. While the three lattice sizes $L = \{6, 12, 18\}$ do not facilitate a rigorous finite-size scaling analysis, the results in Fig. 5 suggest a first-order crystallization transition for all vison crystals, except for the 1/3 flux crystal [73]. Assuming that the transition into the 1/3 flux crystal is continuous, it is conjectured to be in the universality class of the two-dimensional 3-state Potts model, which in turn suggests that the height of the peak in $C(T)/L^2$ should be $\propto L^{\alpha/\nu}$ with critical exponents $\alpha = 1/3$, $\nu = 5/6$, and

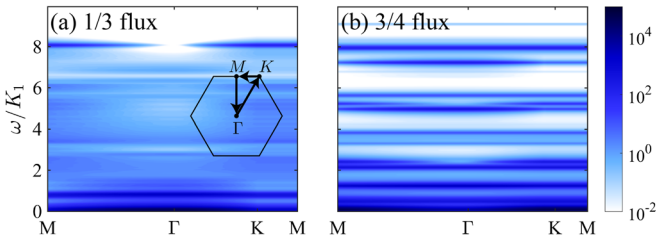

FIG. 4. Dynamical spin structure factor $S_{zz}(\boldsymbol{q}, \omega)$ [60] for the 1/3 flux crystal (a) and the 3/4 flux crystal (b) along the path M-Γ-K-M in the Brillouin zone [see the inset in (a)] via the single-particle approximation of Ref. [69].

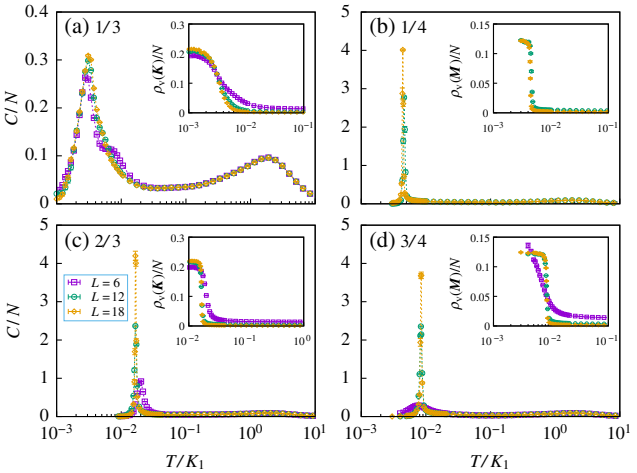

FIG. 5. Temperature dependence of the specific heat and the appropriate static vison structure factor for (a) the 1/3 flux crystal with $K_3 = 0.165K_1$ and $K_3' = 0.19K_1$, (b) the 1/4 flux crystal with $K_3 = 0.165K_1$ and $K_3' = 0.22K_1$, (c) the 2/3 flux crystal with $K_3 = 0.165K_1$ and $K_3' = 0.26K_1$, and (d) the 3/4 flux crystal with $K_3 = 0.19K_1$ and $K_3' = 0.22K_1$ on $L \times L$ lattices ($L = 6$, 12, 18) containing $N = 2L^2$ sites.

$\alpha/\nu = 2/5$ [74]. We note that, for each vison crystal, the critical temperature is $T_c \sim 10^{-2}K_1$.

Discussion.—By considering a natural extension of the honeycomb Kitaev model, we have found a rich spectrum of novel spin-liquid phases that are *not* adiabatically connected to the original Kitaev model, including a fully symmetric π-flux spin liquid, and five distinct symmetry-breaking spin liquids with various degrees of vison crystallization. In the future, it would be interesting to study how an external magnetic field affects our spin liquids. For the Dirac phases, it may generate non-Abelian gapped spin liquids with distinct Chern numbers of the Majorana fermions [1]. For the gapped phases, it may lead to nontrivial finite-field phase transitions between topologically distinct spin liquids.

We thank Arnab Banerjee, Hiroaki Ishizuka, and Johannes Knolle for useful comments on the manuscript. S.-S. Z., Z. W., and C. D. B. are supported by funding from the Lincoln Chair of Excellence in Physics. The work of G. B. H. at ORNL was supported by Laboratory Director's Research and Development funds. This research used resources of the Oak Ridge Leadership Computing Facility, which is a DOE Office of Science User Facility supported under Contract No. DE-AC05-00OR22725.

[1] A. Kitaev, Ann. Phys. (Amsterdam) **321**, 2 (2006).
[2] L. Balents, Nature (London) **464**, 199 (2010).
[3] L. Savary and L. Balents, Rep. Prog. Phys. **80**, 016502 (2017).
[4] G. Jackeli and G. Khaliullin, Phys. Rev. Lett. **102**, 017205 (2009).
[5] J. G. Rau, E. K.-H. Lee, and H.-Y. Kee, Annu. Rev. Condens. Matter Phys. **7**, 195 (2016).
[6] S. Trebst, arXiv:1701.07056.
[7] M. Hermanns, I. Kimchi, and J. Knolle, Annu. Rev. Condens. Matter Phys. **9**, 17 (2018).
[8] Y. Singh and P. Gegenwart, Phys. Rev. B **82**, 064412 (2010).
[9] X. Liu, T. Berlijn, W.-G. Yin, W. Ku, A. Tsvelik, Y.-J. Kim, H. Gretarsson, Y. Singh, P. Gegenwart, and J. P. Hill, Phys. Rev. B **83**, 220403(R) (2011).
[10] Y. Singh, S. Manni, J. Reuther, T. Berlijn, R. Thomale, W. Ku, S. Trebst, and P. Gegenwart, Phys. Rev. Lett. **108**, 127203 (2012).
[11] S. K. Choi, R. Coldea, A. N. Kolmogorov, T. Lancaster, I. I. Mazin, S. J. Blundell, P. G. Radaelli, Y. Singh, P. Gegenwart, K. R. Choi, S.-W. Cheong, P. J. Baker, C. Stock, and J. Taylor, Phys. Rev. Lett. **108**, 127204 (2012).
[12] F. Ye, S. Chi, H. Cao, B. C. Chakoumakos, J. A. Fernandez-Baca, R. Custelcean, T. F. Qi, O. B. Korneta, and G. Cao, Phys. Rev. B **85**, 180403(R) (2012).
[13] R. Comin, G. Levy, B. Ludbrook, Z.-H. Zhu, C. N. Veenstra, J. A. Rosen, Y. Singh, P. Gegenwart, D. Stricker, J. N. Hancock, D. van der Marel, I. S. Elfimov, and A. Damascelli, Phys. Rev. Lett. **109**, 266406 (2012).
[14] S. Hwan Chun, J.-W. Kim, J. Kim, H. Zheng, C. C. Stoumpos, C. D. Malliakas, J. F. Mitchell, K. Mehlawat, Y. Singh, Y. Choi, T. Gog, A. Al-Zein, M. M. Sala, M. Krisch, J. Chaloupka, G. Jackeli, G. Khaliullin, and B. J. Kim, Nat. Phys. **11**, 462 (2015).
[15] S. C. Williams, R. D. Johnson, F. Freund, S. Choi, A. Jesche, I. Kimchi, S. Manni, A. Bombardi, P. Manuel, P. Gegenwart, and R. Coldea, Phys. Rev. B **93**, 195158 (2016).
[16] K. Kitagawa, T. Takayama, Y. Matsumoto, A. Kato, R. Takano, Y. Kishimoto, R. Dinnebier, G. Jackeli, and H. Takagi, Nature (London) **554**, 341 (2018).
[17] K. W. Plumb, J. P. Clancy, L. J. Sandilands, V. V. Shankar, Y. F. Hu, K. S. Burch, H.-Y. Kee, and Y.-J. Kim, Phys. Rev. B **90**, 041112(R) (2014).
[18] L. J. Sandilands, Y. Tian, K. W. Plumb, Y.-J. Kim, and K. S. Burch, Phys. Rev. Lett. **114**, 147201 (2015).
[19] J. A. Sears, M. Songvilay, K. W. Plumb, J. P. Clancy, Y. Qiu, Y. Zhao, D. Parshall, and Y.-J. Kim, Phys. Rev. B **91**, 144420 (2015).
[20] M. Majumder, M. Schmidt, H. Rosner, A. A. Tsirlin, H. Yasuoka, and M. Baenitz, Phys. Rev. B **91**, 180401(R) (2015).
[21] R. D. Johnson, S. C. Williams, A. A. Haghighirad, J. Singleton, V. Zapf, P. Manuel, I. I. Mazin, Y. Li, H. O. Jeschke, R. Valentí, and R. Coldea, Phys. Rev. B **92**, 235119 (2015).
[22] L. J. Sandilands, Y. Tian, A. A. Reijnders, H.-S. Kim, K. W. Plumb, Y.-J. Kim, H.-Y. Kee, and K. S. Burch, Phys. Rev. B **93**, 075144 (2016).
[23] A. Banerjee, C. A. Bridges, J.-Q. Yan, A. A. Aczel, L. Li, M. B. Stone, G. E. Granroth, M. D. Lumsden, Y. Yiu, J. Knolle, S. Bhattacharjee, D. L. Kovrizhin, R. Moessner, D. A. Tennant, D. G. Mandrus, and S. E. Nagler, Nat. Mater. **15**, 733 (2016).
[24] J. A. Sears, Y. Zhao, Z. Xu, J. W. Lynn, and Y.-J. Kim, Phys. Rev. B **95**, 180411(R) (2017).
[25] A. Banerjee, J. Yan, J. Knolle, C. A. Bridges, M. B. Stone, M. D. Lumsden, D. G. Mandrus, D. A. Tennant, R. Moessner, and S. E. Nagler, Science **356**, 1055 (2017).
[26] S.-H. Baek, S.-H. Do, K.-Y. Choi, Y. S. Kwon, A. U. B. Wolter, S. Nishimoto, J. van den Brink, and B. Büchner, Phys. Rev. Lett. **119**, 037201 (2017).
[27] S.-H. Do, S.-Y. Park, J. Yoshitake, J. Nasu, Y. Motome, Y. S. Kwon, D. T. Adroja, D. J. Voneshen, K. Kim, T.-H. Jang, J.-H. Park, K.-Y. Choi, and S. Ji, Nat. Phys. **13**, 1079 (2017).
[28] A. Banerjee, P. Lampen-Kelley, J. Knolle, C. Balz, A. A. Aczel, B. Winn, Y. Liu, D. Pajerowski, J. Yan, C. A. Bridges, A. T. Savici, B. C. Chakoumakos, M. D. Lumsden, D. A. Tennant, R. Moessner, D. G. Mandrus, and S. E. Nagler, npj Quantum Mater. **3**, 8 (2018).
[29] R. Hentrich, A. U. B. Wolter, X. Zotos, W. Brenig, D. Nowak, A. Isaeva, T. Doert, A. Banerjee, P. Lampen-Kelley, D. G. Mandrus, S. E. Nagler, J. Sears, Y.-J. Kim, B. Büchner, and C. Hess, Phys. Rev. Lett. **120**, 117204 (2018).
[30] Y. Kasahara, T. Ohnishi, Y. Mizukami, O. Tanaka, S. Ma, K. Sugii, N. Kurita, H. Tanaka, J. Nasu, Y. Motome, T. Shibauchi, and Y. Matsuda, Nature (London) **559**, 227 (2018).
[31] J. Chaloupka, G. Jackeli, and G. Khaliullin, Phys. Rev. Lett. **105**, 027204 (2010).
[32] H.-C. Jiang, Z.-C. Gu, X.-L. Qi, and S. Trebst, Phys. Rev. B **83**, 245104 (2011).

[33] J. Reuther, R. Thomale, and S. Trebst, Phys. Rev. B **84**, 100406(R) (2011).
[34] C. C. Price and N. B. Perkins, Phys. Rev. Lett. **109**, 187201 (2012).
[35] J. G. Rau, E.-H. Lee, and H.-Y. Kee, Phys. Rev. Lett. **112**, 077204 (2014).
[36] Y. Yamaji, Y. Nomura, M. Kurita, R. Arita, and M. Imada, Phys. Rev. Lett. **113**, 107201 (2014).
[37] Y. Sizyuk, C. Price, P. Wölfle, and N. B. Perkins, Phys. Rev. B **90**, 155126 (2014).
[38] E. Sela, H.-C. Jiang, M. H. Gerlach, and S. Trebst, Phys. Rev. B **90**, 035113 (2014).
[39] I. Rousochatzakis, J. Reuther, R. Thomale, S. Rachel, and N. B. Perkins, Phys. Rev. X **5**, 041035 (2015).
[40] H.-S. Kim, V. Shankar V., A. Catuneanu, and H.-Y. Kee, Phys. Rev. B **91**, 241110(R) (2015).
[41] R. Yadav, N. A. Bogdanov, V. M. Katukuri, S. Nishimoto, J. Van Den Brink, and L. Hozoi, Sci. Rep. **6**, 37925 (2016).
[42] H.-S. Kim and H.-Y. Kee, Phys. Rev. B **93**, 155143 (2016).
[43] S. M. Winter, Y. Li, H. O. Jeschke, and R. Valentí, Phys. Rev. B **93**, 214431 (2016).
[44] B. H. Kim, T. Shirakawa, and S. Yunoki, Phys. Rev. Lett. **117**, 187201 (2016).
[45] L. Janssen, E. C. Andrade, and M. Vojta, Phys. Rev. Lett. **117**, 277202 (2016).
[46] Y. S. Hou, H. J. Xiang, and X. G. Gong, Phys. Rev. B **96**, 054410 (2017).
[47] S. M. Winter, A. A. Tsirlin, M. Daghofer, J. van den Brink, Y. Singh, P. Gegenwart, and R. Valentí, J. Phys. Condens. Matter **29**, 493002 (2017).
[48] A. M. Samarakoon, A. Banerjee, S.-S. Zhang, Y. Kamiya, S. E. Nagler, D. A. Tennant, S.-H. Lee, and C. D. Batista, Phys. Rev. B **96**, 134408 (2017).
[49] K. Ran, J. Wang, W. Wang, Z.-Y. Dong, X. Ren, S. Bao, S. Li, Z. Ma, Y. Gan, Y. Zhang *et al.*, Phys. Rev. Lett. **118**, 107203 (2017).
[50] A. M. Samarakoon, G. Wachtel, Y. Yamaji, D. A. Tennant, C. D. Batista, and Y. B. Kim, Phys. Rev. B **98**, 045121 (2018).
[51] J. S. Gordon, A. Catuneanu, E. S. Sørensen, and H.-Y. Kee, Nat. Commun. **10**, 2470 (2019).
[52] Y.-M. Lu and Y. Ran, Phys. Rev. B **84**, 024420 (2011).
[53] Y.-Z. You, I. Kimchi, and A. Vishwanath, Phys. Rev. B **86**, 085145 (2012).
[54] L. Savary and L. Balents, Phys. Rev. Lett. **108**, 037202 (2012).
[55] E. H. Lieb, Phys. Rev. Lett. **73**, 2158 (1994).
[56] R. Ozawa, S. Hayami, K. Barros, G.-W. Chern, Y. Motome, and C. D. Batista, J. Phys. Soc. Jpn. **85**, 103703 (2016).
[57] C. D. Batista, S.-Z. Lin, S. Hayami, and Y. Kamiya, Rep. Prog. Phys. **79**, 084504 (2016).
[58] R. Ozawa, S. Hayami, and Y. Motome, Phys. Rev. Lett. **118**, 147205 (2017).
[59] In this Letter, "*n*th neighbor" means that the shortest path connecting the two sites consists of n bonds.
[60] See Supplemental Material at http://link.aps.org/supplemental/10.1103/PhysRevLett.123.057201 for extended descriptions of the quadratic Majorana problems and the corresponding nodal structures in the various phases and for detailed results on the magnetic Friedel oscillations and the dynamical spin structure factor, as well as for implementation details of the Monte Carlo simulations.
[61] X.-Y. Song, Y.-Z. You, and L. Balents, Phys. Rev. Lett. **117**, 037209 (2016).
[62] We verified that fluctuations in the phase boundaries due to finite-size effects become negligibly small for lattices larger than 36×36 unit cells.
[63] We verified this statement by running unbiased MC simulations for multiple randomly chosen points within each phase on finite lattices of 12×12 unit cells.
[64] G. E. Volovik, *The Universe in a Helium Droplet* (Oxford University Press, New York, 2003).
[65] M. Hermanns and S. Trebst, Phys. Rev. B **89**, 235102 (2014).
[66] G. B. Halász, N. B. Perkins, and J. van den Brink, Phys. Rev. Lett. **117**, 127203 (2016).
[67] G. B. Halász, B. Perreault, and N. B. Perkins, Phys. Rev. Lett. **119**, 097202 (2017).
[68] J. Knolle, D. L. Kovrizhin, J. T. Chalker, and R. Moessner, Phys. Rev. Lett. **112**, 207203 (2014).
[69] J. Knolle, D. L. Kovrizhin, J. T. Chalker, and R. Moessner, Phys. Rev. B **92**, 115127 (2015).
[70] J. Nasu, M. Udagawa, and Y. Motome, Phys. Rev. Lett. **113**, 197205 (2014).
[71] J. Nasu, M. Udagawa, and Y. Motome, Phys. Rev. B **92**, 115122 (2015).
[72] We average over eight independent runs to estimate the errors.
[73] The height of the peak in $C(T)/L^2$ is proportional to the system volume L^2 for first-order transitions and to $L^{\alpha/\nu}$ for second-order transitions.
[74] M. P. M. den Nijs, J. Phys. A **12**, 1857 (1979).